

Pattern Recognition in Time-Frequency Domain: Selective Regional Correlation and Its Applications

Ervin Sejdić¹ and Jin Jiang²

¹*Bloorview Research Institute and the Institute of Biomaterials and Biomedical Engineering, University of Toronto, Toronto, Ontario, M4G 1R8,*

²*Department of Electrical and Computer Engineering,
The University of Western Ontario, London, Ontario, N6A 5B9,
Canada*

1. Introduction

Pattern recognition is a very powerful tool in automated data analysis and it is widely used in many different applications (Chou & Juang, 2003; Jiang, 1994; Blue et al., 1994; Milosavljević, 1994; Moreels & Smrekar, 2003). However, the application of such a tool can be a difficult task in some cases. For example, in a correlation-type scheme, the basic idea is to correlate the signal being analyzed with a known template or templates (Shiavi, 1999; Scharf, 1991) and make decisions based on the magnitude of the correlation coefficients, which is between 0 and 1. In practice, these extreme values are seldom achieved due to corrupting signals/noise that can affect the accuracy of pattern matching and subsequently lead to errors in classification (Kil & Shin, 1996). The corrupting signals may also bear some resemblance to the template being matched. This is particularly true if the pattern of interest is a non-stationary transient signal. Furthermore, it is well known that traditional time domain correlation-based pattern recognition methods do not fully utilize the frequency characteristics of the template and the signal being analyzed. Hence, such methods perform poorly when applied to transient signals. To overcome these difficulties, a scheme known as selective regional correlation (SRC) has been developed (Sejdić & Jiang, 2007). It has been shown that if a template has bandlimited characteristics, significant improvement in the performance of pattern recognition can be readily made by a relatively simple pre-processing of the signal and the template in the time-frequency domain (Sejdić & Jiang, 2007). The redundant representation of a 1D signal in a 2D time-frequency domain can provide an additional degree of freedom for signal analysis. Such pre-processing effectively separates the intertwined time domain features of the signal, allowing the important characteristics to be exposed in the time-frequency domain, resulting in more effective pattern matching. Hence, correlation between the signal being analyzed and the template needs to be conducted only in selected regions of interest in the time-frequency domain.

An overview of the theoretical developments behind the SRC is provided in this chapter along with some recent results. The performance of the scheme is briefly reviewed and compared with that of the general correlation technique through the analysis of a set of

synthetic short duration transients. The results have shown that the SRC enhances the resolution and accuracy for classification of transient signals significantly. The technique described herein may be of significance in many applications where correlation-based techniques have traditionally been used. The technique has already been applied to classification of heart sounds (Sejdić & Jiang, 2007), and to classification of a faulty machine tool positioning drive (Rehorn et al., 2006). In both cases, the SRC convincingly outperforms the general correlation based technique.

The theoretical background of the SRC is covered in Section 2, whereas Section 3 illustrates its performance using a set of synthetic signals. In Section 4, the application of SRC to heart sound analysis is reviewed, while in Section 5 the review of the application of SRC to detect a specific fault in a machine tool positioning drive is presented. Finally, conclusions are drawn in Section 6.

2. Mathematical developments behind SRC

The decision of a correlation-based pattern classifier depends on the output value of the correlator and thus its performance will be directly related to the quality of the correlation process. Hence, the essence of SRC is to represent a 1D time domain signal in a 2D time-frequency representation to reveal its true characteristics for more accurate pattern matching as depicted in Fig. 1.

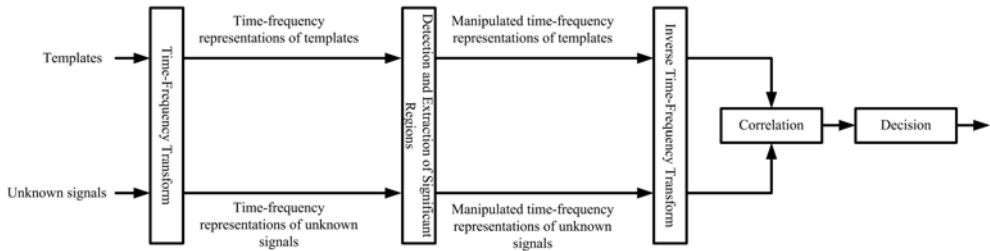


Fig. 1. A block diagram of SRC.

A time-frequency transform of a bandlimited template, $p(t)$, can be represented as:

$$Tp(t, \omega) = \int_{-\infty}^{+\infty} p(\tau)\phi_{t,\omega}(\tau)d\tau \tag{1}$$

and

$$Tp(t, \omega) \equiv 0 \quad \forall \quad t \notin [t_1, t_2] \quad \omega \notin [\omega_1, \omega_2] \tag{2}$$

where t_1 and t_2 are the lower and the upper limits of the time band, ω_1 and ω_2 are the lower and the upper limits of the frequency band and $\phi_{t,\omega} \in L^2(\mathbb{R})$ (sometimes known as the time-frequency atom) is a well-concentrated function in time and frequency (Mallat, 1999). The time-frequency atoms considered in this chapter are given in Table 1.

Furthermore, assume that there exists a finite duration signal, $s(t)$, composed of elements that are similar to the template, $s^{(1)}(t)$, and elements different from the template, $s^{(2)}(t)$. Thus, the following signal decomposition is in order:

$$Ts(t, \omega) = Ts^{(1)}(t, \omega) \cup Ts^{(2)}(t, \omega) \tag{3}$$

Method	$\phi_{\tau,\omega}(t)$
Short-time Fourier transform (STFT) (Mallat, 1999)(Gröchenig, 2001)	$e^{-j\omega t}g(t - \tau)$ where g is a window function.
Continuous wavelet transform (CWT) (Mallat, 1999)(Daubechies, 1992)	$\frac{1}{\sqrt{s}}\psi\left(\frac{t-\tau}{s}\right)$ where ψ is a mother wavelet.
S-transform(Stockwell et al., 1996)(Pinnegar, 2001)	$e^{-j\omega t}g\left(\frac{t-\tau}{\omega}\right)$ where g is a Gaussian window.

Table 1. The time-frequency atoms in different transforms.

where

$$Ts^{(1)}(t, \omega) = Ts(t, \omega) \quad t \in [t_1, t_2] \quad \text{and} \quad \omega \in [\omega_1, \omega_2] \quad (4)$$

and

$$Ts^{(2)}(t, \omega) = \overline{Ts(t, \omega) \cap Ts^{(1)}(t, \omega)} \quad (5)$$

with $Ts^{(1)}(t, \omega)$ and $Ts^{(2)}(t, \omega)$ denoting time-frequency representations of $s^{(1)}(t)$ and $s^{(2)}(t)$, respectively. To effectively obtain $Ts^{(1)}(t, \omega)$ from $Ts(t, \omega)$, different 2D windows can be used (Sejdić & Jiang, 2007):

$$Ts^{(1)}(t, \omega) = Ts(t, \omega) \cdot W(t, \omega) \quad t \in [t_1, t_2] \quad \text{and} \quad \omega \in [\omega_1, \omega_2]. \quad (6)$$

where $W(t, \omega)$ is a 2D window in the time-frequency domain.

Assuming that $s^{(1)}(t)$ is similar to pattern $p(t)$, then the following statement is true:

$$\max \left[|corr(s^{(1)}(t), p(t))| \right] > \max \left[|corr(s(t), p(t))| \right] \quad (7)$$

where $\max \left[|corr(x(t), y(t))| \right]$ is defined as:

$$\max \left[|corr(x(t), y(t))| \right] = \max_{\tau} \left[\left| \frac{\int_{-\infty}^{\infty} x(t)y(t + \tau)dt}{\sqrt{\int_{-\infty}^{\infty} x(t)^2dt} \sqrt{\int_{-\infty}^{\infty} y(t)^2dt}} \right| \right] \quad (8)$$

and $x(t)$ and $y(t)$ are assumed to be zero-mean signals. This statement is possible due to the fact that $s^{(2)}(t)$ lies in the frequency and the time bands outside those of pattern $p(t)$. For a complete proof, please refer to (Sejdić & Jiang, 2007).

The concept of the SRC is also applicable to a multiple templates case, but the templates must be mutually exclusive. Hence, the templates $p_1(t), \dots, p_m(t)$ with the time-frequency representations $Tp_1(t, \omega), \dots, Tp_m(t, \omega)$ would have

$$Tp_1(t, \omega) \cap Tp_2(t, \omega) \cap Tp_3(t, \omega) \cap \dots \cap Tp_m(t, \omega) = \emptyset \quad (9)$$

However, if

$$Tp_k(t, \omega) \cap Tp_l(t, \omega) \neq \emptyset \quad \text{for} \quad k \neq l \quad (10)$$

for some k and l , it is necessary to introduce a mutually exclusive template in order to reduce the peak correlation coefficient when the signal does not match the template. This exclusivity is represented in the time-frequency domain as:

$$Tp_k^{(1)}(t, \omega) = Tp_k(t, \omega) - (Tp_k(t, \omega) \cap Tp_l(t, \omega)) \quad (11)$$

and the corresponding template can be found by multiplying a time-frequency decomposition of the template $Tp_k^{(1)}(t, \omega)$ with a 2D window, $W_k(t, \omega)$, with appropriate time and frequency bands, and inverting back to the time domain.

Based on (9)-(11), it can be stated that any template can be expressed as a sum of mutually exclusive terms, $p^{(1)}(t)$, and $p^{(2)}(t)$, that is,

$$p(t) = p^{(1)}(t) + p^{(2)}(t) \quad (12)$$

where $p^{(2)}(t)$ would be zero for disjoint templates. Therefore, if the signal $z(t)$ does not contain the template $p(t)$, the SRC using $p^{(1)}(t)$ will produce a smaller correlation coefficient, namely,

$$\max [|\text{corr}(z(t), p(t))|] > \max [|\text{corr}(z(t), p^{(1)}(t))|] \quad (13)$$

where $\max [|\text{corr}(x(t), y(t))|]$ is as defined in (8). In addition, it is necessary to have the following constraint:

$$\int_{-\infty}^{\infty} \int_{-\infty}^{\infty} |Tp^{(1)}(t, \omega)| d\tau d\omega \gg \int_{-\infty}^{\infty} \int_{-\infty}^{\infty} |Tp^{(2)}(t, \omega)| d\tau d\omega \quad (14)$$

For a complete proof, please refer to (Sejdić & Jiang, 2007).

The mutual exclusivity of the templates is the main reason why SRC is a superior pattern matching technique to general correlation-based approaches. The exclusivity of the templates is only possible by introducing a redundant representation of the signal, such as the one in time-frequency domain.

3. Comparative performance evaluation of SRC using synthetic test signals

In this section, the performance of the SRC compared to general correlation is reviewed through a set of test signals. Having this objective in mind, it is prudent to understand that most of the real-world patterns are not limited to a single frequency, but rather are often a sum of transients containing different frequencies. These frequencies can vary with time and are often within a certain frequency band. Therefore, in order to mimic practical conditions, the following templates and signals have been selected in this evaluation:

$$p_1(t) = \begin{cases} p_o(t) + \sin(2\pi 95t) + \sin(2\pi 102t) \\ \quad + \sin(2\pi 105t) + \sin(2\pi 110t) & 0.4 \leq t \leq 0.6 \\ p_o(t) & \text{otherwise} \end{cases} \quad (15)$$

$$p_2(t) = \begin{cases} p_o(t) + \sin(2\pi 60t) + \sin(2\pi 67t) \\ \quad + \sin(2\pi 70t) + \sin(2\pi 75t) & 0.58 \leq t \leq 0.74 \\ p_o(t) & \text{otherwise} \end{cases} \quad (16)$$

$$s_{1_i}(t) = \begin{cases} p_o(t) + \sum_{k=1}^{k=6} \sin(\lfloor 2\pi 250R \rfloor t) & 0.04 + \frac{\lfloor 30R \rfloor}{500} \leq t \leq 0.26 + \frac{\lfloor 20R \rfloor}{500} \\ p_o(t) + \sum_{k=1}^{k=4} \sin(2\pi(95 + \lfloor 15R \rfloor)t) & 0.40 + \frac{\lfloor 20R \rfloor}{500} \leq t \leq 0.60 + \frac{\lfloor 20R \rfloor}{500} \\ p_o(t) + \sum_{k=1}^{k=6} \sin(\lfloor 2\pi 250R \rfloor t) & 0.84 + \frac{\lfloor 20R \rfloor}{500} \leq t \leq 0.90 + \frac{\lfloor 25R \rfloor}{500} \\ p_o(t) & \text{otherwise} \end{cases} \quad (17)$$

$$s_{2_i}(t) = \begin{cases} p_o(t) + \sum_{k=1}^{k=6} \sin(\lfloor 2\pi 250R \rfloor t) & 0.04 + \frac{\lfloor 30R \rfloor}{500} \leq t \leq 0.26 + \frac{\lfloor 20R \rfloor}{500} \\ p_o(t) + \sum_{k=1}^{k=4} \sin(2\pi(60 + \lfloor 15R \rfloor)t) & 0.58 + \frac{\lfloor 20R \rfloor}{500} \leq t \leq 0.74 + \frac{\lfloor 20R \rfloor}{500} \\ p_o(t) + \sum_{k=1}^{k=6} \sin(\lfloor 2\pi 250R \rfloor t) & 0.84 + \frac{\lfloor 20R \rfloor}{500} \leq t \leq 0.90 + \frac{\lfloor 25R \rfloor}{500} \\ p_o(t) & \text{otherwise} \end{cases} \quad (18)$$

where

$$p_o(t) = 0.8[\sin(2\pi 10t) + \sin(2\pi 15t) + \sin(2\pi 18t)] \quad (19)$$

and $R \sim \mathcal{N}(0, 1)$ simulates the uncertainties in the signals with $t \in [0, 1]$. $\lfloor x \rfloor$ represents the greatest integer function, which gives the largest integer less than or equal to x .

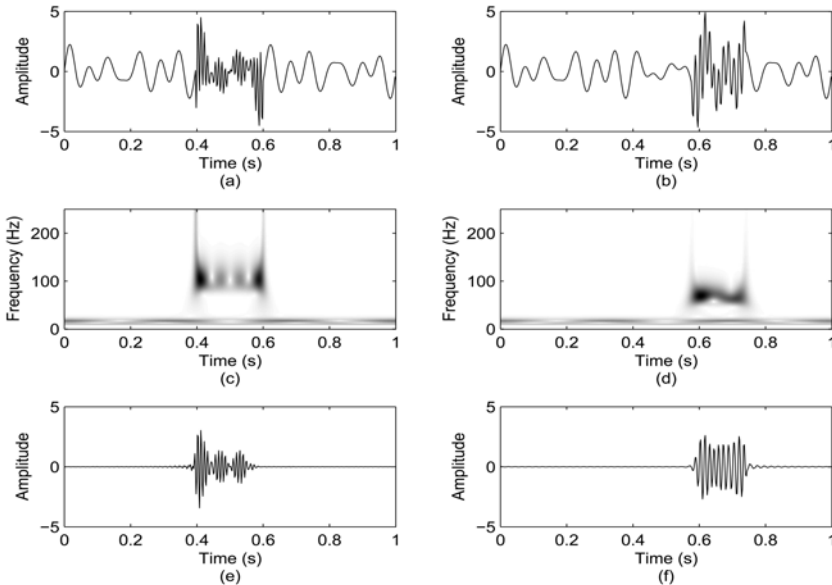


Fig. 2. Time-domain and time-frequency domain representations of dual templates: (a) time domain representation of template of the first template; (b) time domain representation of template of the second template; (c) time-frequency domain representation of the first template; (d) time-frequency domain representation of the second template; (e) time domain representation of the first template after pre-processing; (f) time domain representation of the second template after pre-processing.

The templates are depicted by the top two graphs in Fig. 2. They have the same low frequency content, but the transients that occur in the templates represent two different phenomena as described by (15) and (16). The time-frequency representations of the templates are obtained according to (1) using the S-transform. Their main characteristics can be summarized by the following equations:

$$Tp_1(t, \omega) = \begin{cases} \Omega_{p_{11}} = \{(t, \omega) : t \in [0.38, 0.62], \omega \in [50, 160] \text{ Hz}\} \\ \Omega_{p_{12}} = \{(t, \omega) : t \in [0, 1], \omega \in [8, 26] \text{ Hz}\} \end{cases} \quad (20)$$

$$Tp_2(t, \omega) = \begin{cases} \Omega_{p_{21}} = \{(t, \omega) : t \in [0.55, 0.77], \omega \in [40, 120] \text{ Hz}\} \\ \Omega_{p_{22}} = \{(t, \omega) : t \in [0, 1], \omega \in [8, 26] \text{ Hz}\} \end{cases} \quad (21)$$

with the regions of support including the bands in which the amplitude of time-frequency representations is greater than or equal to one percent of its maximum amplitude. The overlapped time-frequency areas are excluded by windowing in order to form the mutually exclusive templates $p_1^{(i)}(t)$ and $p_2^{(i)}(t)$. The time domain representations of these mutually exclusive templates are shown in the bottom two graphs of Fig. 2.

Furthermore, ten thousand test signals, $s_i(t)$ where $i = 1 \dots 10000$, were constructed according to (17) and (18); with half of the signals containing the patterns similar to $p_1(t)$ and the other half similar to $p_2(t)$. Since each of these signals can contain either of the templates, a window function is needed to capture all the variations. In this case, a window, $W_{gd}(t, \omega)$ was designed to support the region $\Omega_{gd} = \{(t, \omega) : t \in [0.38, 0.77], \omega \in [40, 160] \text{ Hz}\}$.

The correlations were performed by using general correlation and the SRC, and the results are presented in Table 2. These results represent an average of 10000 trials. In Table 2, ρ_M represents the situation where the signal matches the template as specified, while ρ_{NM} represents the situation where the signal does not match the template. Also, $\varphi = \rho_M - \rho_{NM}$ denotes the resolution, and the error percentage (EP) is calculated according to $EP = MC/(MC + CC) * 100\%$, where CC and MC represent the number of correct classifications and misclassifications, respectively.

Method		ρ_M	ρ_{NM}	φ	EP
SRC	STFT	0.5827	0.0823	0.5004	0.0001%
	CWT	0.4856	0.3207	0.1649	1.9600%
	S-transform	0.5835	0.0789	0.5046	0.0000%
General Correlation		0.6127	0.5625	0.0502	19.4900%

Table 2. Comparison of the peak correlation coefficients for SRC and general correlation.

The SRC performed significantly better than general correlation as shown in Table 2, especially when the S-transform and STFT are used. Furthermore, the error percentage for the SRC-based classifier is only 0-2%, while for the conventional correlation-based classifier is almost 20%.

To be useful in practice, any pattern recognition scheme should possess a high degree of sensitivity to the template, and be robust to slight variations in the signals being analyzed. Therefore, the robustness of the SRC has been examined by stretching and shrinking the

signals at three different levels. The results of such an analysis are presented in Table 3 and these represent an average of 10000 trials with the S-transform used as a time-frequency representation. Also, each trial represents the mean value of the two operations: expansion and compression.

Amount of expansion and compression				
	0%	10%	15%	20%
ρ_M	0.5835	0.5064	0.4057	0.2834
ρ_{NM}	0.0789	0.0848	0.1197	0.1611
φ	0.5046	0.4215	0.2860	0.1223
EP	0.0000%	0.0000%	0.0002%	7.7400%

Table 3. Robustness of the proposed scheme to expansion and compression.

As demonstrated, slight variations in the range of 0 - 15% have no major effect on the performance of the SRC based pattern classifier since the accuracy remains almost the same as shown in Table 3, even though the resolution has decreased by a factor of 2. However, deterioration in performance can be seen for variations larger than 20%. Therefore, the SRC can be considered very robust.

4. Heart sound classification by SRC based scheme

Despite numerous advances and decades of declining death rates, cardiovascular diseases (CVDs) remain the leading cause of death worldwide; contributing to more than 17 million deaths or one-third of all deaths each year. CVD is becoming increasingly prevalent in developing countries and, by 2010, CVDs are expected to kill more people in developing countries than infectious diseases according to World Health Organization (W. H. Organization, 2006). Fortunately, clinical experience has shown that heart sounds analysis can be an effective tool to noninvasively diagnose some of the diseases (Khan, 1996; Ravin, 1977), since they provide clinicians with valuable diagnostic and prognostic information concerning the heart valves and hemodynamics. Heart auscultation is an important technique for detecting abnormal heart behaviour before using more sophisticated techniques such as the ECG or ultrasound imaging (Durand & Pibarot, 1995; Erickson, 1997; Obadiat, 1993).

Heart sounds are the result of a sudden closure of the heart valves at different phases of the cardiac contraction. They are non-stationary, non-deterministic signals that carry information about the anatomical and physiological state of the heart. Heart sounds are result of the interplay of dynamic events associated with the contraction and relaxation of atria and ventricles, valve movements and blood flow (Ravin, 1977; Durand & Pibarot, 1995). Each heart beat consists of at least the first heart sound (S1) and second heart sound (S2). S1 occurs at the onset of the ventricular contraction during closure of the mitral and the tricuspid valves. It indicates the beginning of the ventricular systole. The intensity of S1 is closely related to that event. S1 consists of four components with frequency range 70-110 Hz. It starts with a low-frequency component (M1) synchronous with the first myocardial contraction after the onset of rise in the ventricular pressure. The second component (T1) has a higher frequency and is caused by tension of the left ventricular structures; contraction of myocardium and deceleration of blood. The third occurs at the time of opening of the aortic

valve and is related to sudden acceleration of blood into the ventricular walls. The fourth component is due to turbulence in the blood flow in the ascending aorta. The intensity of S1 varies depending on the following factors: position of auscultation, the anatomy of chest, the vigor of ventricular contraction, valve position at the onset of ventricular contraction, and the pathological alternation of the valve structure (Erickson, 1997; Horovitz, 1988). S2 marks the end of ventricular systole and the beginning of ventricular relaxation following the closure of the aortic and the pulmonary valves. Therefore, two different components could be heard in S2, and those are A2 and P2. These are produced by vibrations initiated by the closure of the aortic and the pulmonary semilunar valves, and by sudden cessation of backflow of the blood (Khan, 1996; Ravin, 1977).

A heart problem known as mitral stenosis is caused by a rheumatic heart disease in the majority of cases. This leads to narrowing of the mitral valve. As a result, it slows down the free flow of blood from the left atrium to the left ventricle. Blood returning from the lungs backs up in the left atrium and in the lungs. As a consequence, there is a gradual increase in pressure in the left atrium and in the pulmonary (lung) circulation. This condition can eventually lead to enlargement of the left atrium, weakening of the atrium wall, and gradually result in more serious conditions due to the reduced ability to propel blood efficiently (Horovitz, 1988). Mitral stenosis is very often manifested through a heart sound known as the opening snap (OS); a short, sharp sound occurring in the early diastole. It is caused by the abrupt halting at its maximal opening of an abnormal atrioventricular valve and the OS usually occurs 0.08-0.10 s after S2 (Ravin, 1977; Erickson, 1997). However, the difficulty, as shown in the top two graphs of Fig. 3, lies in the fact that the OS sounds very similar to the third heart sound (S3), which is often heard in normal children or young adults. When S3 is heard in individuals over the age of 40, it usually reflects cardiac disease characterized by ventricular dilatation, decreased systolic function, and elevated ventricular diastolic filling pressure. It is generally difficult to distinguish these two sounds without going through proper training (Khan, 1996; Ravin, 1977; Erickson, 1997).

The objective of this study is to examine the suitability of the SRC for classification of aforementioned conditions. For full details of the study, please refer to (Sejdić & Jiang, 2007). For the purpose of clear illustration, one signal from each group is selected as the template for that group and both templates are depicted in the top two graphs of Fig. 3. As shown, most of the energy associated with an OS is concentrated between 50 and 300 Hz, while that of S3 lies between 30 and 150 Hz (boxed regions in Fig. 3). The templates have to be decoupled, since there is an overlap in some frequency ranges between the two signals. Based on the numerical analysis, it is concluded that the template for OS, $p_{OS}(t)$, should have frequency range between 120 and 300 Hz and its time duration should be around 50 ms, while the template for S3, $p_{S3}(t)$, should have frequency range between 30 and 70 Hz and its time duration should be near 100 ms. Since the signal being analyzed could contain either OS or S3, the frequency band for the window is chosen as $\omega \in [30 \ 300]$ Hz.

Similar to the previous case, the performance of the SRC is again evaluated by comparing it with that of the general correlation, and the results are shown in Table 4. These results represent an average of thirty trials. σ_M , σ_{NM} and σ are the standard deviations of ρ_M , ρ_{NM} and φ , respectively. A comparison of the values of these two states shows that the SRC performs significantly better than the general correlation. Furthermore, T-test is used to inspect whether ρ_M and ρ_{NM} are statistically different for classifiers based both on SRC and

general correlation. The analysis concludes that the null hypothesis (the means are equal) can be rejected at the 0.05 significance level for the SRC based classifier, but not for the classifier based on the general correlation.

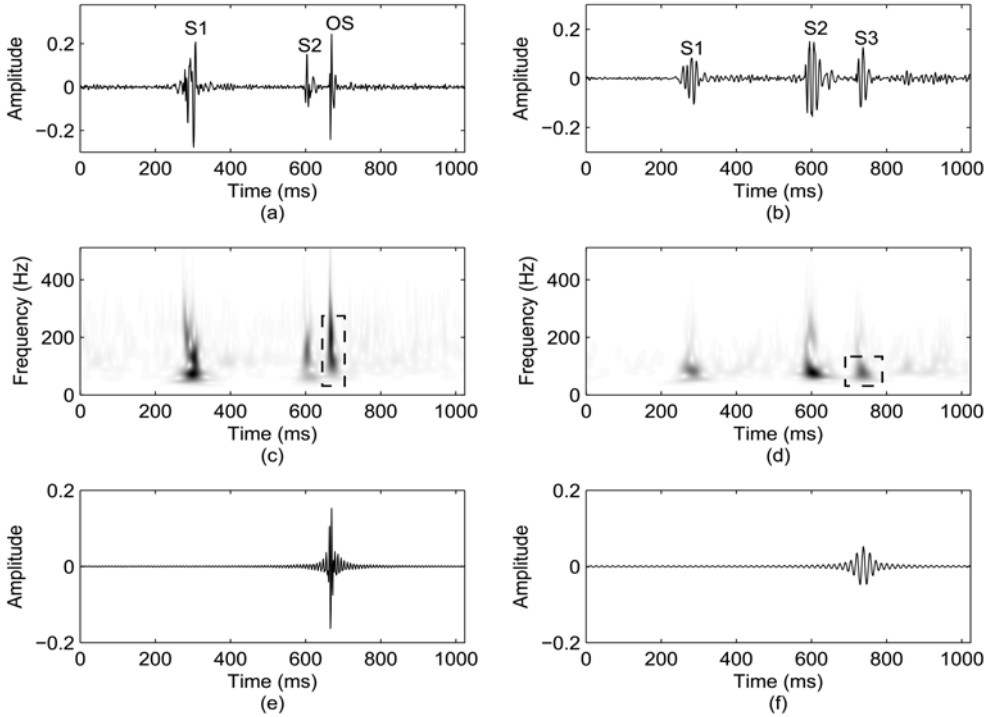


Fig. 3. Time domain, time-frequency domain representations and the templates: (a) time domain representation of heart sounds with a typical OS; (b) time domain representation of heart sounds with a typical S3; (c) time-frequency representation of (a); (d) time-frequency representation of (b); (e) the template based on the typical OS; (f) the template based on the typical S3.

Method	ρ_M	σ_M	ρ_{NM}	σ_{NM}	φ	σ_φ	EP
SRC STFT	0.5533	0.1627	0.2413	0.0942	0.3120	0.2263	10.00%
CWT	0.6731	0.1546	0.5248	0.1097	0.1483	0.1347	16.67%
S-transform	0.4905	0.1043	0.1661	0.0708	0.3244	0.1582	6.670%
General Correlation	0.3477	0.1087	0.3352	0.0562	0.0126	0.1122	56.67%

Table 4. Heart sound classification with different techniques.

5. Fault diagnosis of servo drives in machine tools

There are many potential sources for mechanical failure in the main positioning system of a machine tool including DC servomotor brush seizing, drive belt wear or stretching, and wear in the bearings and lead screws. Each of these problems exhibits a specific

characteristic signature. These signatures can be used for machine condition monitoring (MCM). The key is to identify a set of features that correspond unambiguously to either the healthy mode or possible faulty modes of the machine. Such features can be found in vibration signals of the axes during machining. By comparing the measured data to the failure signature, the health of the machine tool positioning drives can be determined.

This study focuses on brush seizing faults in a DC servo motor drive that controls the position of the spindle block on the machine tool. This fault originates from the design and construction of the brush holders, which are plastic and often warp with exposure to heat and lubricant. Whenever this happens, the spindle block experiences excessive vibration. When one of the servos is faulty, the axis jumps along the guideways rather than moving smoothly. Experience has shown that this type of fault always leads to failure.

It has been found that, for a healthy spindle, there are no fixed patterns in the vibration signals. However, periodic phenomena arise when a fault starts to develop in the system (Rehorn, 2003). These phenomena become much more apparent in the time-frequency domain because they often appear as transient spikes of short durations. It is difficult to detect them either in the time domain or in the frequency domain alone. This is because both the healthy and the faulty drives contain energy in the same frequency bands. However, there are increased periodic fluctuations with energy concentrated in the 20-200 Hz band when the system is faulty. Thus, a faulty system will exhibit a regular pattern of spikes in this frequency range, while a healthy one will not (Rehorn, 2003).

Templates are selected using three different 2D windows, with each of the windows isolating a feature in the time-frequency domain which exists for a range $R = \{(t, \omega) : t \in [540, 630], \omega \in [20, 200]\}$ (Rehorn et al., 2006). The selection of a specific template with the rectangular window in the X direction is shown in Fig. 4. The upper graph depicts the S-transform of the entire vibration signal, $TV_F(t, \omega)$, and the boxed region on the graph represents the area covered by the 2D window. The middle graph displays the windowed and isolated feature of interest in the time-frequency domain, $TV_{F1}(t, \omega)$. The bottom graph shows the corresponding time domain signal, $v_{F1}(t)$, that is used in SRC.

SRC improves the ability to distinguish between similar and dissimilar patterns beyond conventional correlation by improving the resolution for different states of the system. The results are presented in Tables 5-8. The values for ρ_M and ρ_{NM} are the average values over twelve tests. From these results, several interesting observations can be made. The highest values of φ for a specified time-frequency method are generally in Z direction, although this is not the case for the S-transform. Also, changing the time-frequency method used has a more pronounced effect on the SRC resolution than do the shape and type of the window employed for feature extraction. It should also be noted that the S-transform has achieved the best resolution among all three time-frequency methods used, with the STFT being the runner up. The CWT has the poorest resolution of the three methods tested in the X and Y directions, but its resolution is equal to, or even better than, the others in Z direction. Of the three windows considered, the Kaiser yields the highest resolution while the Gaussian window performs the worst.

By comparing the values in Tables 5 - 7, with those in Table 8, the values generated by general correlation for similar events are much smaller than those calculated using time-frequency methods and SRC in the given direction. General correlation of similar events

generates only 10% similarity at the most; well below the value of ρ_{NM} produced by any of the time-frequency methods. This is mainly due to the non-stationary nature of the vibration signals in this case. The resolution of general correlation is extremely poor as well, and never exceeds 5%, while any combination of time-frequency method and 2D window with SRC results in very high resolution between the two states. Thus, an MCM system that relies on general correlation will not be able to perform as effectively as the one based on time-frequency methods and SRC.

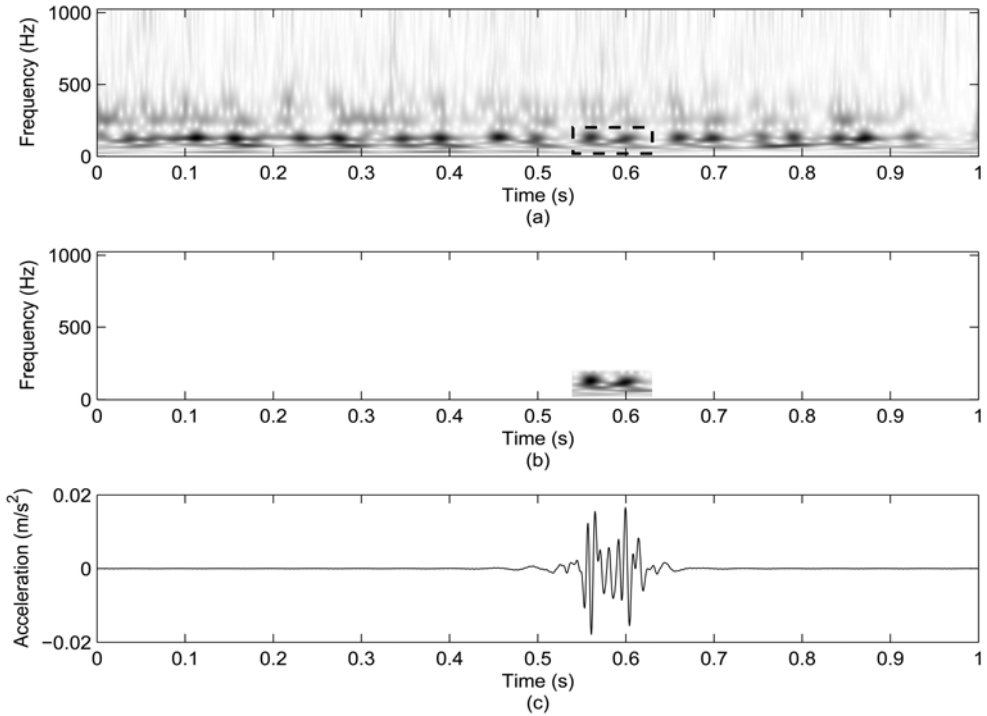


Fig. 4. Template signal selection from the S-transform of a faulty drive: (a) time-frequency representation of a faulty drive; (b) extracted template in time-frequency domain; and (c) the template in the time domain.

Directions	Selective Regional Correlation								
	STFT			CWT			S-transform		
	X	Y	Z	X	Y	Z	X	Y	Z
ρ_M	0.4531	0.5177	0.6701	0.2994	0.1688	0.7343	0.5522	0.6557	0.5981
ρ_{NM}	0.2413	0.2342	0.3298	0.1399	0.1075	0.2574	0.1810	0.1762	0.1433
φ	0.2118	0.2835	0.3403	0.1595	0.0613	0.4769	0.3712	0.4795	0.4548

Table 5. Performance of SRC using a 2D rectangular window.

Directions	Selective Regional Correlation								
	STFT			CWT			S-transform		
	X	Y	Z	X	Y	Z	X	Y	Z
ρ_M	0.4836	0.5521	0.6918	0.3467	0.1978	0.7960	0.5847	0.6951	0.6230
ρ_{NM}	0.3141	0.3064	0.3849	0.2206	0.1489	0.3965	0.2768	0.2524	0.2851
φ	0.1695	0.2457	0.3069	0.1261	0.0489	0.3995	0.3079	0.4427	0.3379

Table 6. Performance of SRC using a 2D Gaussian window.

Directions	Selective Regional Correlation								
	STFT			CWT			S-transform		
	X	Y	Z	X	Y	Z	X	Y	Z
ρ_M	0.6171	0.6643	0.7243	0.4823	0.1931	0.8210	0.6211	0.7184	0.6673
ρ_{NM}	0.3318	0.3397	0.3322	0.2631	0.1143	0.3829	0.2293	0.2219	0.3049
φ	0.2853	0.3246	0.3912	0.2192	0.0788	0.4381	0.3918	0.4965	0.3624

Table 7. Performance of SRC using a 2D Kaiser window.

Directions	X	Y	Z
ρ_M	0.0652	0.0560	0.1002
ρ_{NM}	0.0581	0.0285	0.0536
φ	0.0071	0.0275	0.0466

Table 8. Performance of classifier using general correlation.

6. Conclusion

In this chapter, a recently developed technique for pattern classification based on time-frequency decomposition is presented. The essence of the scheme is that the correlation between the observed signal and the template is conducted only in selected regions of interest in the time-frequency domain. The results of two applications have indicated conclusively that the proposed technique provides a consistent improvement over the traditional correlation-based pattern classification schemes.

7. References

- W. Chou and B. H. Juang, Eds., *Pattern Recognition in Speech and Language Processing*. London: CRC Press, 2003.
- J. Jiang, "Design of reconfigurable control systems using eigenstructure assignments," *International Journal of Control*, vol. 59, pp. 395-410, 1994.
- J. L. Blue, G. T. Candela, P. J. Grother, R. Chellappa, C. L. Wilson, and J. D. Blue, "Evaluation of pattern classifiers for fingerprint and OCR applications," *Pattern Recognition*, vol. 27, no. 4, pp. 485-501, Apr. 1994.

- A. Milosavljević, "Algorithmic significance, mutual information, and DNA sequence comparisons," in *Proceedings of the Data Compression Conference*, Mar. 29-31, 1994, p. 457.
- P. Moreels and S. Smrekar, "Watershed identification of polygonal patterns in noisy SAR images," *IEEE Transactions on Signal Processing*, vol. 12, no. 7, pp. 740-750, Jul. 2003.
- R. Shiavi, *Introduction to Applied Statistical Signal Analysis*, 2nd ed. San Diego: Academic Press, 1999.
- L. L. Scharf, *Statistical Signal Processing: Detection, Estimation, and Time Series Analysis*. Addison Wesley, 1991.
- D. H. Kil and F. B. Shin, *Pattern Recognition and Prediction with Applications to Signal Characterization*. Woodbury, NY: AIP Press, 1996.
- E. Sejdić and J. Jiang, "Selective regional correlation for pattern recognition," *IEEE Transactions on Systems, Man and Cybernetics - Part A*, vol. 37, no. 1, pp. 82-93, Jan. 2007.
- A. G. Rehorn, E. Sejdić, and J. Jiang, "Fault diagnosis in machine tools using selective regional correlation," *Mechanical Systems and Signal Processing*, vol. 20, no. 5, pp. 1221-1238, Jul. 2006.
- S. G. Mallat, *A Wavelet Tour of Signal Processing*, 2nd ed. San Diego: Academic Press, 1999.
- K. Gröchenig, *Foundations of Time-Frequency Analysis*. Boston: Birkhäuser, 2001.
- I. Daubechies, *Ten Lectures on Wavelets*. Philadelphia: Society for Industrial and Applied Mathematics, 1992.
- R. G. Stockwell, L. Mansinha, and R. P. Lowe, "Localization of the complex spectrum: The S-transform," *IEEE Transactions on Signal Processing*, vol. 44, no. 4, pp. 998-1001, Apr. 1996.
- R. Pinnegar, "The generalized S-transform and TT-transform, in one and two dimensions," Ph.D. dissertation, The University of Western Ontario, London, Ontario, Canada, Sep. 2001.
- W. H. Organization, "Cardiovascular disease: prevention and control," Apr. 2006. [Online]. Available: <http://www.who.int/dietphysicalactivity/publications/facts/cvd/en/>
- M. G. Khan, *Heart Disease Diagnosis and Therapy: A Practical Approach*. Baltimore: Williams and Wilkins, 1996.
- A. Ravin, *Auscultation of the Heart*, 3rd ed. Chicago: Year Book Medical Publishers, 1977.
- L. Durand and P. Pibarot, "Digital signal processing of the phonocardiogram: Review of the most recent advancements," *Critical Reviews in Biomedical Engineering*, vol. 23, no. 3-4, pp. 169-219, 1995.
- B. Erickson, *Heart Sounds and Murmurs: A Practical Guide*, 3rd ed. St. Louis: Mosby-Year Book, 1997.
- M. Obadiat, "Phonocardiogram signal analysis: Techniques and performance analysis," *Journal of Medical Engineering and Technology*, vol. 17, no. 6, pp. 221-227, Nov./Dec. 1993.
- E. Horovitz, *Heart Beat: A Complete Guide to Understanding and Preventing Heart Disease*. Los Angeles, CA: Health Trend Publishing, 1988.

- A. G. Rehorn, P. E. Orban, and J. Jiang, "Vibration-based machine condition monitoring with attention to the use of time-frequency methods," in *Proc. of SPIE Conference on Intelligent Manufacturing*, vol. 5263, Providence, RI, USA, Oct. 29, 2003, pp. 10-21.